HAL open science

Mechanical behaviour of a stone masonry bridge assessed using an implicit discrete element method

A. Rafiee, Marc Vinches

To cite this version:

A. Rafiee, Marc Vinches. Mechanical behaviour of a stone masonry bridge assessed using an implicit discrete element method. Engineering Structures, 2013, 48, pp.739-749. 10.1016/j.engstruct.2012.11.035 . hal-03260504

HAL Id: hal-03260504

https://imt-mines-ales.hal.science/hal-03260504v1

Submitted on 5 Jun 2023

HAL is a multi-disciplinary open access archive for the deposit and dissemination of scientific research documents, whether they are published or not. The documents may come from teaching and research institutions in France or abroad, or from public or private research centers.

L'archive ouverte pluridisciplinaire **HAL**, est destinée au dépôt et à la diffusion de documents scientifiques de niveau recherche, publiés ou non, émanant des établissements d'enseignement et de recherche français ou étrangers, des laboratoires publics ou privés.

Mechanical behaviour of a stone masonry bridge assessed using an implicit discrete element method

A. Rafiee [a], M. Vinches [b,*]

[a] Mining Engineering Department, University of Zanjan, Iran
[b] Centre des Matériaux de Grande Diffusion, Ecole des Mines d'Alès, France

A B S T R A C T

The aim of this study is to investigate the effect of different types of static loadings on the mechanical behaviour of a standard arch bridge and a masonry stone bridge in real scale. The mechanical analyses are performed using the Non-Smooth Contact Dynamic method (NSCD) known as an implicit discrete element method. After a brief description of the NSCD method, the stability state analysis is carried out over a classic stone arch in order to demonstrate the efficiency of this numerical method to reveal the diverse collapse mechanisms happening in the masonry structures under several static loading conditions. For the analysis of a real masonry structure, the roman stone bridge of the Pont Julien in Vaucluse (South of France) is studied, based on site measurements, under an academic loading, to show the capacity of the method to take into account heterogeneous loading patterns.

Keywords:
Non-Smooth Contact Dynamics method
Stone bridge stability
Stone arch stability
Discrete elements
Deformable discrete elements
Massonry structures

1. Introduction

The masonry stone arch bridge is one of the oldest constructions; this structure makes use of the high compressive strength of rock blocks to transmit the loads to the ground [1]. On the contrary, rock blocks cannot resist to a high amount of the shearing load, therefore the strength of stone arch bridges against shear and tension is very low. The stability state analysis and failure mechanism of masonry arch structures is a complex task, and has to take into account diverse loads applied to the structure, including its own weight. In other words, the predictability of masonry arch structures mechanical behaviour can be considered with caution [2]. Conservation and restoration of historical structures are always a challenge to modern practitioners even if significant research advances have recently occurred [3]. Times shows that historical masonry structures collapsed due to natural disaster such as earthquakes, or floods. As a result in order to understand the influences of these actions over the masonry structure, safety assessment and mechanical analysis of historical buildings are often necessary [3].

One can notice that, even nowadays, masonry arch bridges in a majority of countries are considered as the main part of national road and rail network bridges. As a result, their assessment, especially for the structures in use, becomes a necessary task [4]. On the other hand, for some countries stone arch bridges are considered as part of the cultural heritage. In these cases also, their more detailed analysis is of interest in view of their preservation, and/or restoration and reinforcement [5].

A number of numerical approaches exist for assessing the mechanical behaviour of the masonry structures. Masonry structures in most cases include a heterogeneous material composed of blocks, with various shapes and sizes, separated by joints [6]. A stone bridge consists of stone blocks and mortar joints. In some cases the mortar does not exist as it is the case in almost all roman large stone course bridges. By considering the discontinuous nature of masonry structures, computational methods which take into account this feature are more suitable to investigate their mechanical behaviour. A method based on a discontinuous conception such as the discrete element method (DEM) considers a masonry structure as a collection of distinct blocks, each block being able to move. Different types of computational techniques such as discrete element based approaches, discontinuous deformation analysis (DDA) and combined finite element/discrete element method are nowadays used to investigate the mechanical behaviour of masonry structures [7]. The three-dimensional limit analysis is also successfully applied to investigate masonry construction failure mechanism by considering different mechanical behaviours and contact interaction laws [8–10].

In the current study, the mechanical behaviour of stone masonry arch bridges is investigated by an implicit discrete element method known as Non-Smooth Contact Dynamics method (NSCD).

* Corresponding author. Tel.: +33 4 66 78 50 00; fax: +33 4 66 78 53 65.
E-mail addresses: ali_rafiee@znu.ac.ir (A. Rafiee), marc.vinches@mines-ales.fr (M. Vinches).

The NSCD method is incorporated in the open platform program LMGC90 [11]. This code allows us to model the geometrically complex masonry structures, made of rigid or deformable bodies, with complex mechanical behaviour (elasto-plastic, damaged materials) or interactions (frictional and cohesive contacts). LMGC90 [11] is based on a hybrid or extended FEM–DEM discretization, using various numerical strategies, such as molecular dynamics MD or NSCD. The NSCD method is applied in the first phase of this study to investigate the behaviour of a classic stone arch bridge in two and three dimensions, and afterwards a roman stone bridge in realistic scale is studied under static and quasi-static loading conditions. But before beginning the modelling stages, a brief explanation is presented in order to introduce the NSCD method and the LMGC90 code.

2. The Non-Smooth Contact Dynamics method

Included in the group of the "discrete element methods" (DEM) introduced by P. Cundall, the NSCD method is distinguishable from the original DEM due to the following items:

- An implicit scheme for integrating the time discretized dynamical equation.
- A non-regularized interaction law (Signorini unilateral contact and Coulomb dry friction)

As it is the case with other distinct element methods, the possibility for finite element discretization in order to fit the mechanical behaviour of rock blocks (elastic, elasto-plastic, visco-plastic behaviour) is also available with the NSCD method, based on mathematical formulation of non-smooth dynamics, extended and developed by Jean and Moreau [12–19]. One of the important characteristics of the NSCD method is its capability to resolve frictional contact problems without introducing artificial penalization parameters or damping. The Coulomb friction law and rigid contact condition is perfectly taken into account in this method. The NSCD method does not involve small interpenetrations between particles as with a customary DEM method, and the algorithm used is unconditionally stable due to an implicit discretization [20].

The frictional contact relationship between two adjacent bodies can be explained as follows [21]. We can consider these two bodies sufficiently close to come into contact in the point **P** shown schematically in Fig. 1. Then we define a normal vector $\overrightarrow{N}$ which points from one body considered as the antagonist to the other body, considered as a candidate to contact and a tangential vector $\overrightarrow{T}$, which also gives the other axis of the local coordination system in the contact point. In this way, local variables are introduced in order to define a frictional contact law:

The relative velocity of **P** with respect to O':

$$U = (U_T, U_N) \tag{1}$$

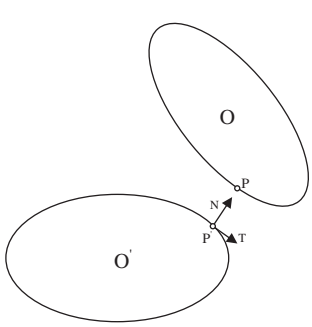

Fig. 1. Schematic local frame for an antagonist and a candidate body at a potential contact between two particles.

The reaction force exerted by O' on O:

$$R = (R_T, R_N) \tag{2}$$

and the gap distance is defined by: $g = \overline{P'P}$.

The Signorini condition takes into account three basic conditions that establish the first unilateral constraint in this technique:

- Impenetrability: $g \geqslant 0$.
- No attraction acts between bodies: $R_N \geqslant 0$.

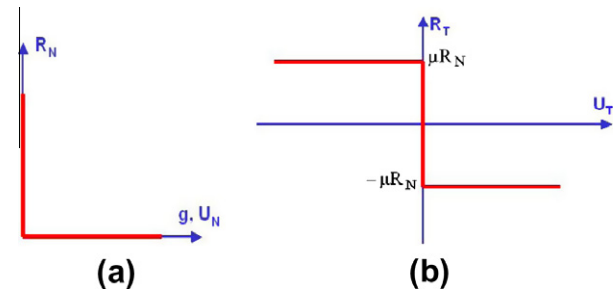

Fig. 2. Contact interaction: (a) the Signorini law and (b) Coulomb dry friction law.

Table 1
Mechanical properties: (a) average mechanical properties measured for three rock samples from limestone quarry of Estaillades [27] and (b) mechanical parameters used for the numerical analyses in the current study.

	Density (kg/m^3)	Porosity (%)	Young's modulus (MPa)	Poisson's ratio
(a)				
Sample 1	1860	33	12,000	0.22
Sample 2	1860	33	14,900	0.23
Sample 3	1860	33	12,800	0.24

	Density (kg/m^3)	Young's modulus (MPa)	Poisson's ratio
(b)			
Parameters used in this study	1860	13,000	0.23

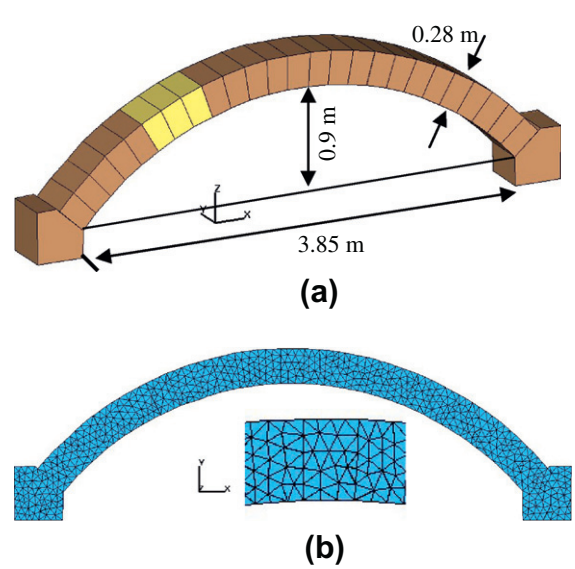

Fig. 3. Classic stone arch bridge, the arch part is composed of 25 blocks [28]: (a) 3D rigid model with a thickness of 0.40 m and (b) 2D deformable (deformable discrete element) model and a close-up image of triangular mesh elements.

– Once the bodies are no longer in contact, the reaction force vanishes [9,10]:

$$g > 0 \Rightarrow R_N = 0 \tag{3}$$

These relations are summarized schematically in the graph shown in Fig. 2a. It should be added that in the case of a cohesive condition between two bodies in the contact state, the cohesive force is added to R_N, but this force is set to zero once the two bodies lose their contact. In other words, a potential contact point between two particles has the following dynamic content: as long as the gap distance between them remains positive, no contact force is activated and R_N is zero; once there is no gap distance, normal contact force is mobilized at the contact point [22].

The second unilateral constraint is the Coulomb dry friction law that establishes the two following conditions Fig. 2b:

– Calculating the friction force with respect to Coulomb's law: this force is limited by Coulomb's cone: $\|R_T\| \leqslant \mu R_N$, where μ is the friction coefficient.
– In the case of the sliding condition, the friction force is considered in the opposite direction of sliding and its value is equal to μR_N:

$$U_T^+ \neq 0 \Rightarrow R_T = \mu R_N \frac{U_T^+}{\|U_T^+\|} \tag{4}$$

This law can be used to treat frictional contact problems for deformable or rigid bodies. It should be noted that more complicated friction laws can be added to this technique. After describing the unilateral constraints taken into account in this technique, we now explain the dynamic equations that are employed to formulate the motion process [13,14]. The dynamic equation of a body in consideration of contact (but without shock phenomenon) can be written in the following form:

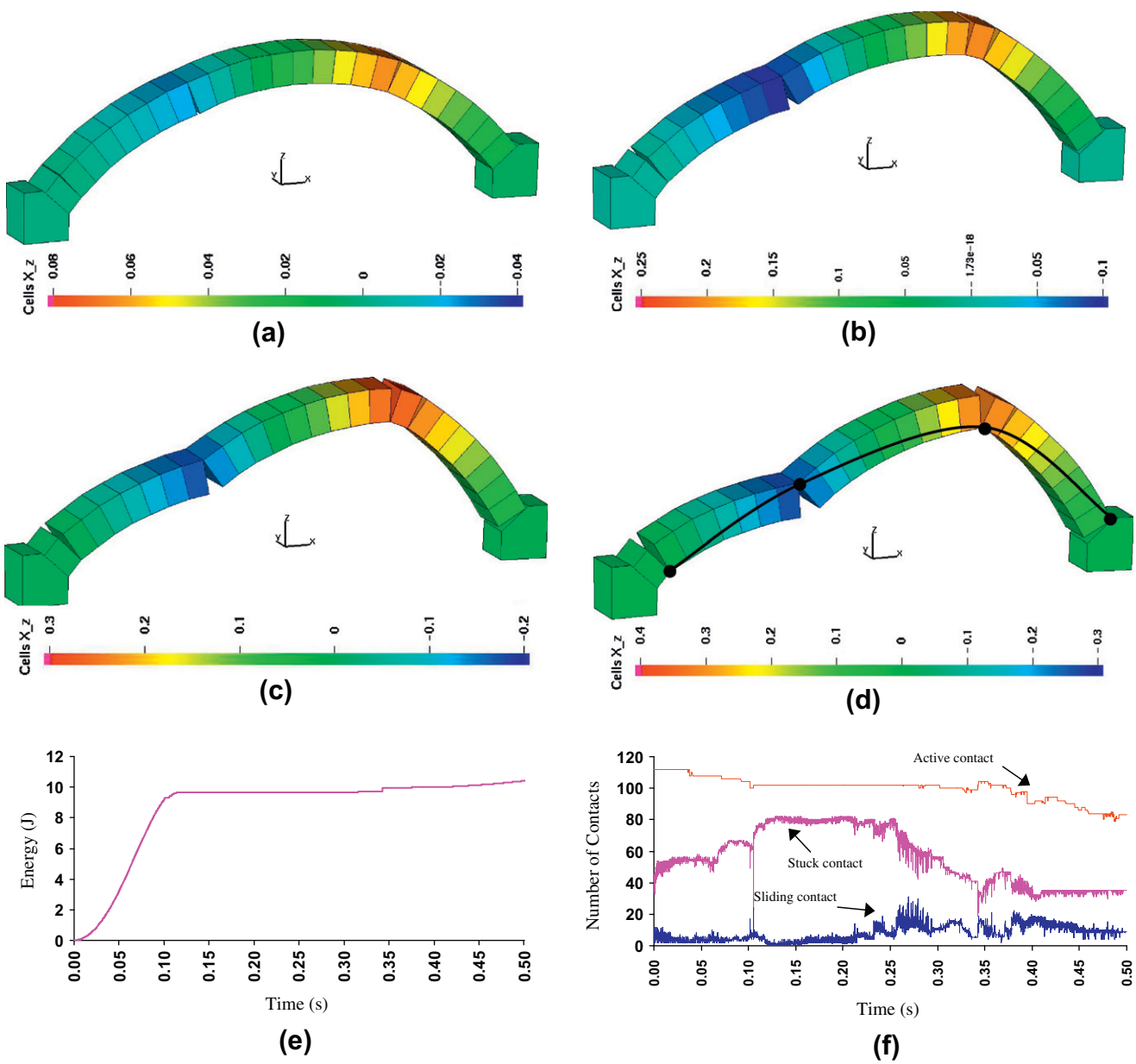

Fig. 4. Results obtained for the 3D rigid model (a–d) four snapshots of the vertical displacement distribution over the model in meter respectively for 0.1, 0.2, 0.25 and 0.3 s of the calculation time, (e) evolution of the cumulative dissipated energy in Joule during the calculation, and (f) change in the number of contacts, including sliding, stuck and all active contacts.

$$M\dot{u} = F(q, u, t) + P(t) + r \tag{5}$$

where M is the mass matrix; $F(q, u, t)$ represents internal forces; q is the representative of some parameters for example, the position of the centre of gravity of a rigid body, the rotation parameters of this body or the displacements of the nodes of a finite element mesh; u is the velocity function; r indicates the contribution of the unknown contact forces; and $P(t)$ denotes the external forces.

In the NSCD method the basic interaction laws, explained previously, are considered as non-smooth laws in terms of multi-mappings. The dynamic equation must be discretized by a low order implicit algorithm due to the non-smoothness of the velocity function. Therefore, by considering a time interval $[t_i,\ t_f]$ with length h, the following equation can be yielded:

$$\begin{cases} M(u_f - u_i) = \int_{t_i}^{t_f} (F(q, u, s) + P(s))ds + hr_f \\ q_f = q_i + \int_{t_i}^{t_f} uds \\ hr_f = \int_{t_i}^{t_f} rdv \end{cases} \tag{6}$$

where hr_f, an unknown of the problem, represents the total contact impulse during the time interval. In fact, the main unknowns in the NSCD technique are the relative velocities $U = H^{*}u_f$ between contact boundaries at some overlapping moments with the time steps and average reaction impulses $hr = HhR$ over the time steps (H denotes the linear transition agent). These last two relations allow the transition between the global and local scales. Relative speeds are connected to the local reactions R by the kinematic relations: the laws of Signorini and Coulomb, as described above (for detailed explanations see [12–19,22]). The LMGC90 code is based on the NSCD method and was developed in the Montpellier University mechanical and civil engineering laboratory. This code has been used to study the behaviour of granular materials such as the segregation or compaction phenomena, or railway ballast fatigue. The valuable feature of the LMGC90 is its large range of contact laws already implemented and its ability to consider more complex surface interactions such as cohesion [20]. We intend to use this code for modelling masonry arch structures in this study. It should be mentioned that the NSCD method has been applied to study granular materials, masonry structures and rock slope stability analysis [22–26]. In Ref. [26], one can analyse the comparisons made over the results obtained by the LMGC90 code, limit analysis and finite element method for several classic simple masonry wall models extracted from Refs. [9,10]. The purpose of performing these comparisons was to demonstrate that the results obtained by LMGC90 code are realistic and comparable with other known numerical method and experimental results.

3. Numerical analysis

In the current study, two phases of numerical modelling are presented: first, on a stone arch, then on a real historical masonry bridge. In order to introduce the NSCD method and LMGC90 code, the failure mechanism of a simple stone arch is firstly investigated. The mechanical properties of the stone used for both models are obtained from mechanical tests performed on limestone samples of the Estaillades quarry situated near to the roman stone bridge [27]. Table 1a shows the results of three mechanical tests made on limestone block. Three cores, 70 mm in diameter, and 140 mm high, are extracted from one limestone block in three orthogonal directions in order to take account its slight anisotropies. The stone blocks of this limestone quarry and the roman masonry bridge have the same mechanical and material properties. On the basis of the performed tests, the needed mechanical parameters are extracted for the numerical analyses, for the classic arch and the roman masonry bridge (Table 1). In the case of rigid models, only the rock density is used and for the models with deformable elements, the Young's modulus and the Poisson ratio are also taken into account (Table 1b).

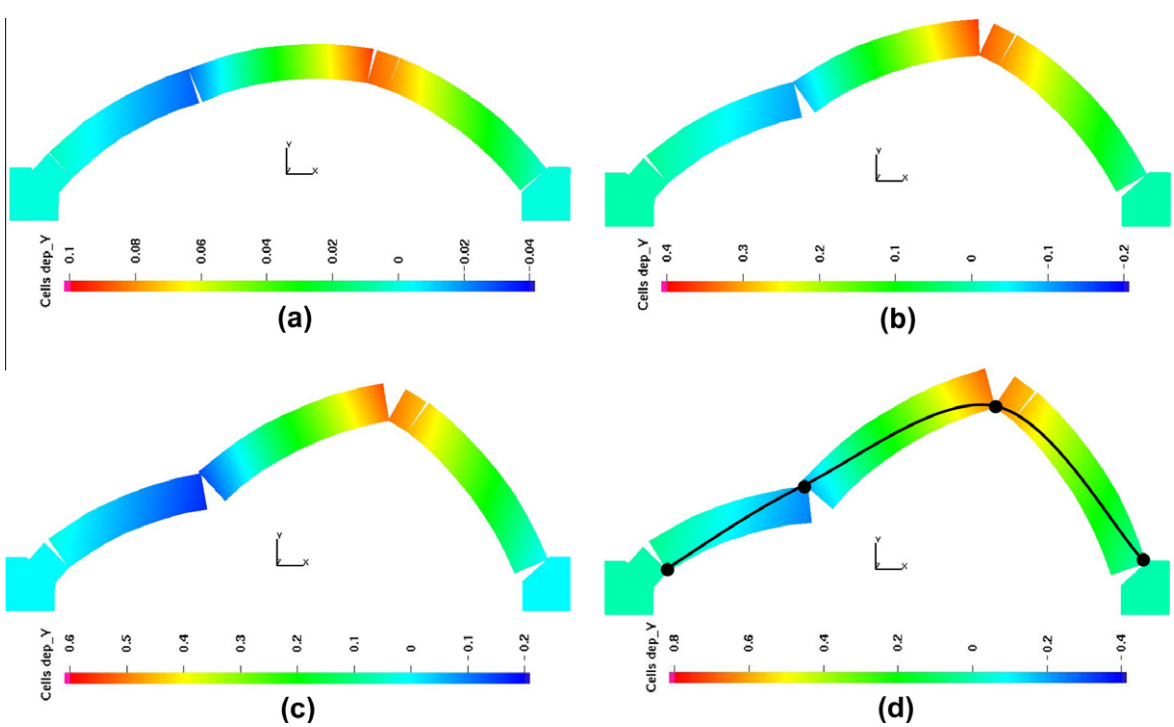

Fig. 5. Results obtained for the 2D deformable model (a–d) four snapshots of the vertical displacement distribution over the model in meter respectively for 0.1, 0.2, 0.25 and 0.3 s of the calculation time.

3.1. Classic stone arch modelling

In the first stage of numerical modelling by the NSCD method, the mechanical behaviour of a classic arch bridge is investigated in two and three dimensions. Fig. 3 illustrates the geometry of a simple classical arch bridge used to show the application and efficiency of the NSCD method for studying the failure mechanism of masonry structures. The arch geometry used in this study is a typical masonry arch bridge [28]. The mechanical behaviour of the model is investigated under static vertical load applied by increasing the density of three blocks shown in Fig. 3a by a different colour. These three blocks are considered to be 100 times denser than the other blocks which have a density of 1860 kg/m^3 (Table 1b). One can notice that a vertical load can be also applied directly to any block of the model statically and dynamically, but in order to have the least imposed changes between the 3D rigid and 2D deformable models the simplest way of static loading is chosen. In other words, the 2D deformable and 3D rigid models are loaded completely in identical ways, so the comparison of their results can be easily made.

The cohesive contact law is applied for this classic arch model: a Coulomb law for which the status at the beginning of calculation is a cohesive status. The normal and tangential cohesion thresholds for this model are respectively 10 kPa and 7 kPa, and the Mohr–Coulomb cone has an opening angle φ so that $\tan(\varphi) = coht/cohn$ where *coht* is the tangential cohesion threshold and *cohn* refers to the normal cohesion. The static friction coefficient at this stage is considered equal to 0.7. Once a cohesive contact is broken; the contact will switch to a dynamic dry friction contact behaviour with the coefficient of friction equal to 0.6.

The results obtained for the 3D rigid model are illustrated in Fig. 4. As can be seen in Fig. 4a–d, the four hinged failure mechanism is obviously distinguishable for this classic arch bridge loaded approximately at the quarter of its span, these hinge points are illustrated in Fig. 4d. It should be noted that this 3D model is composed by undeformable blocks in contact with cohesive Coulomb law. These four snapshots (Fig. 4a–d) show the state of the arch at different instances of the calculation. During the calculation, the cumulative energy dissipated in the model is recorded and illustrated in Fig. 4e. This graph presents the amount of the energy dissipated by breaking cohesive contacts, friction and shocks within the model. As can be observed, this energy shows a high increase for the first 0.1 s, and then remains more or less unchanged. The change of the number of contacts in the model is also monitored during the computation. The graph in Fig. 4f shows the change in the different type of contacts including stuck and sliding contact, and also the total of active contacts. As can be seen, the number of active and stuck contacts decreases by increasing the instability inside the model, and, accordingly, the number of sliding contacts increases.

The mechanical behaviour of this arch is also investigated by considering the deformable blocks in a 2D model. The deformable model consists of 27 discrete block meshed by 1069 triangular elements. The stone blocks in this deformable model are considered

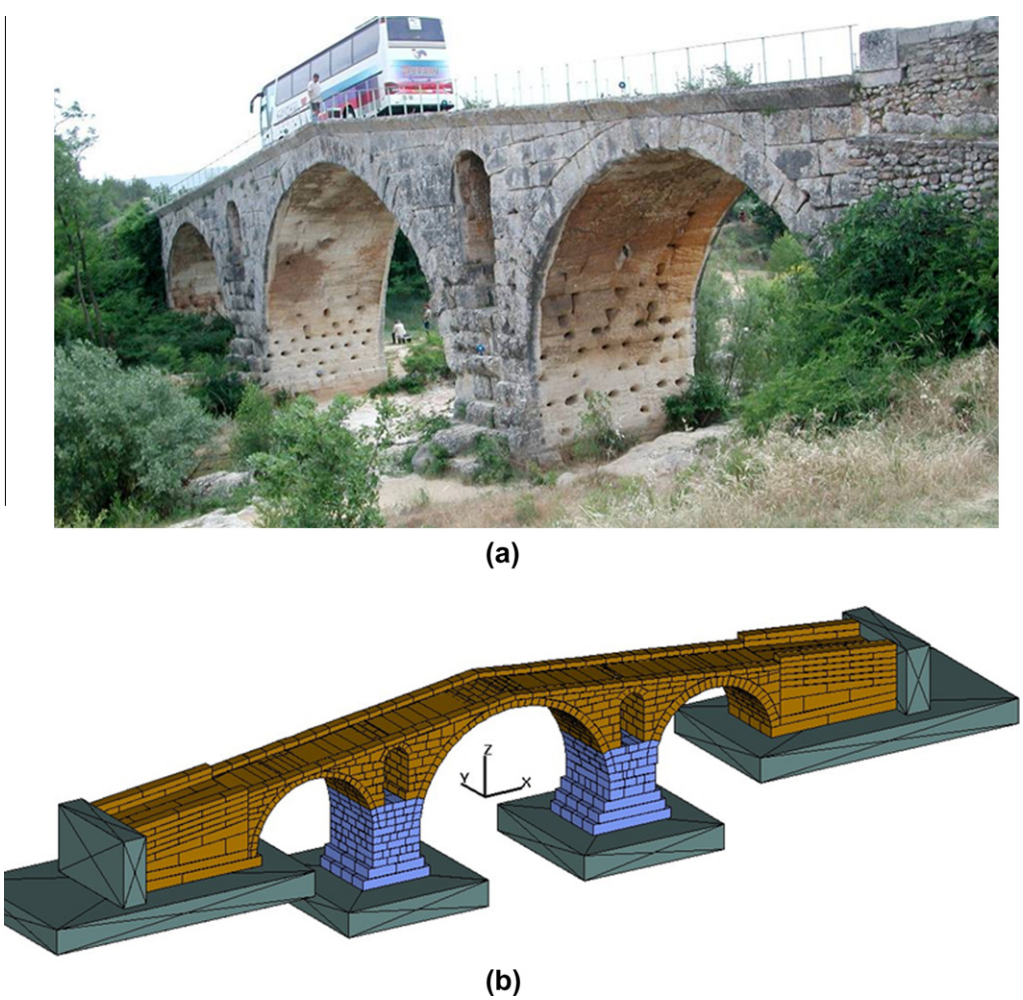

Fig. 6. Pont Julien: (a) view of three spans of the Julien stone bridge and (b) 3D model with 1219 rigid blocks and boundary condition considered for this model.

to have a Young's modulus of 13 GPa, and a Poisson's ratio of 0.23 (Table 1b). The contact condition law and the vertical loading are same as in the 3D rigid model. Fig. 5 shows the four snapshot images of the results obtained for the deformable model. The similar failure mechanism can be observed for this model, with four hinge points (Fig. 5d). The failure mechanism is globally the same for both models, but the 2D deformable model is more time consuming. Consequently, as the global behaviour of the structure does not seem to be different, the 3D rigid model, being faster to compute is preferred, and will be used in similar cases of large stone block masonries subjected to mechanical loads.

3.2. Pont Julien bridge modelling

In this part of the study, the mechanical behaviour of a roman bridge called Pont Julien in the Vaucluse region located in south-east of France is investigated [6]. The Pont Julien is a Roman stone arch bridge over the river of Calavon and dates from 3 BC. It was located on the via Domitia, an important Roman road. It has a total length of 85 m, a width of 5.9 m and it is composed of three arches with span of 10.2 m, 16 m and 10.2 m each (Fig. 6a). This study is focused on the mechanical behaviour of the central part of this bridge under static and quasi-static loading states. Fig. 6b shows

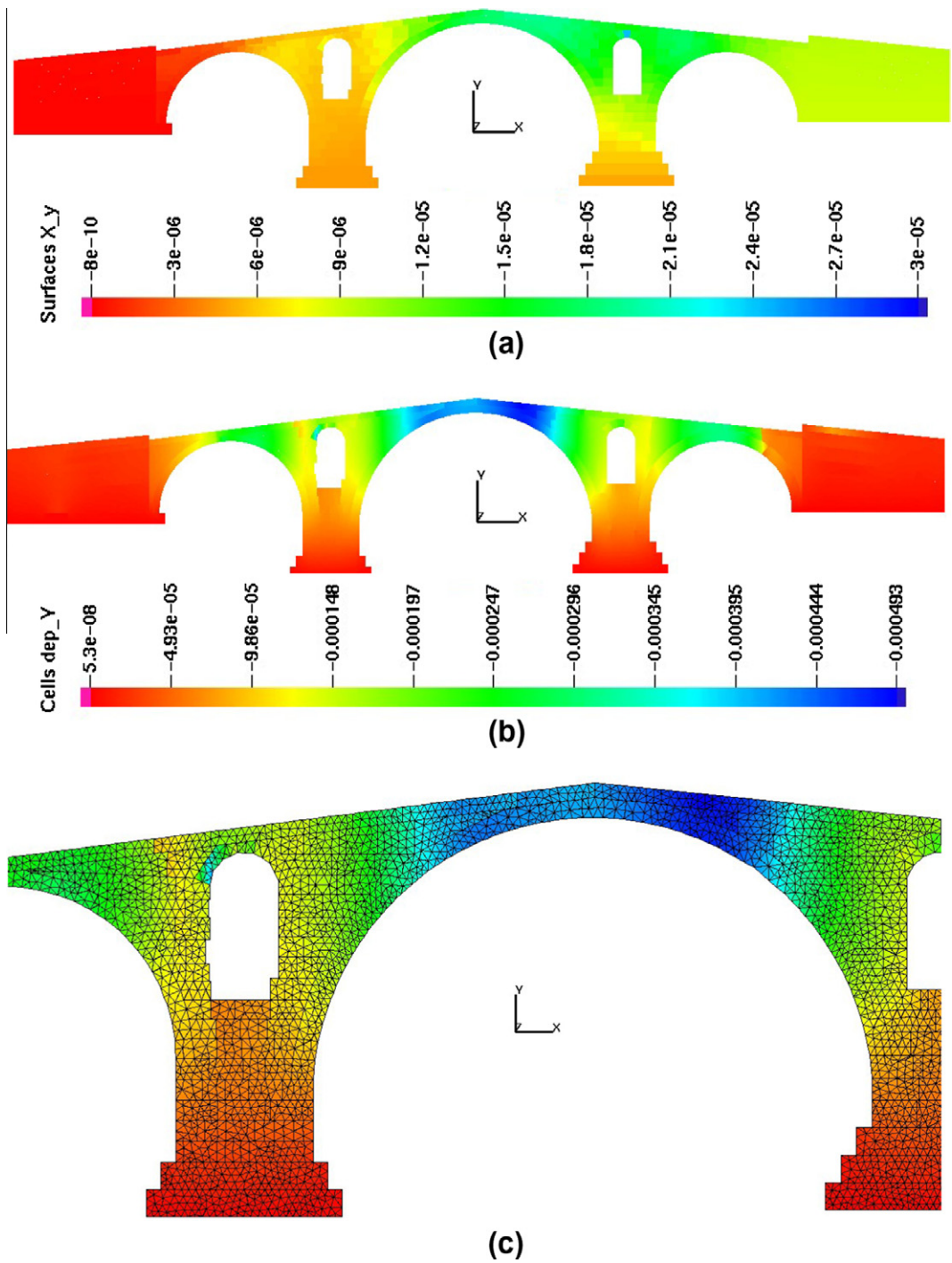

Fig. 7. Julien bridge: (a and b) vertical displacement in meter for static state calculated respectively for 2D rigid and deformable models and (c) close-up view of the 2D deformable model with blocks meshed using triangular elements.

a 3D model of the Julien bridge created by 1219 blocks and also the boundary conditions considered during the modelling phase. The bridge is considered fixed laterally and in the base part of the model by the ground. Two central pillars are shown in two different colours, because below part of them will be loaded by a lateral force which increases incrementally with time. These parts are considered to be under muddy water during floods, as a result their apparent densities are considered to be 760 kg/m^3 in the coming models. This inundated part for each pillar is considered to be 6 m high, divided into three 2 m high levels. The lateral forces applied on each pillar can be uniform over these three levels or not. The lateral forces are used in the following models to study the mechanical behaviour of the bridge under out-of-plane loading. One of these types of loading can partly represent the case of a flooding condition; however flooding has its complexities such as sudden changes in water heights, water velocity, and water

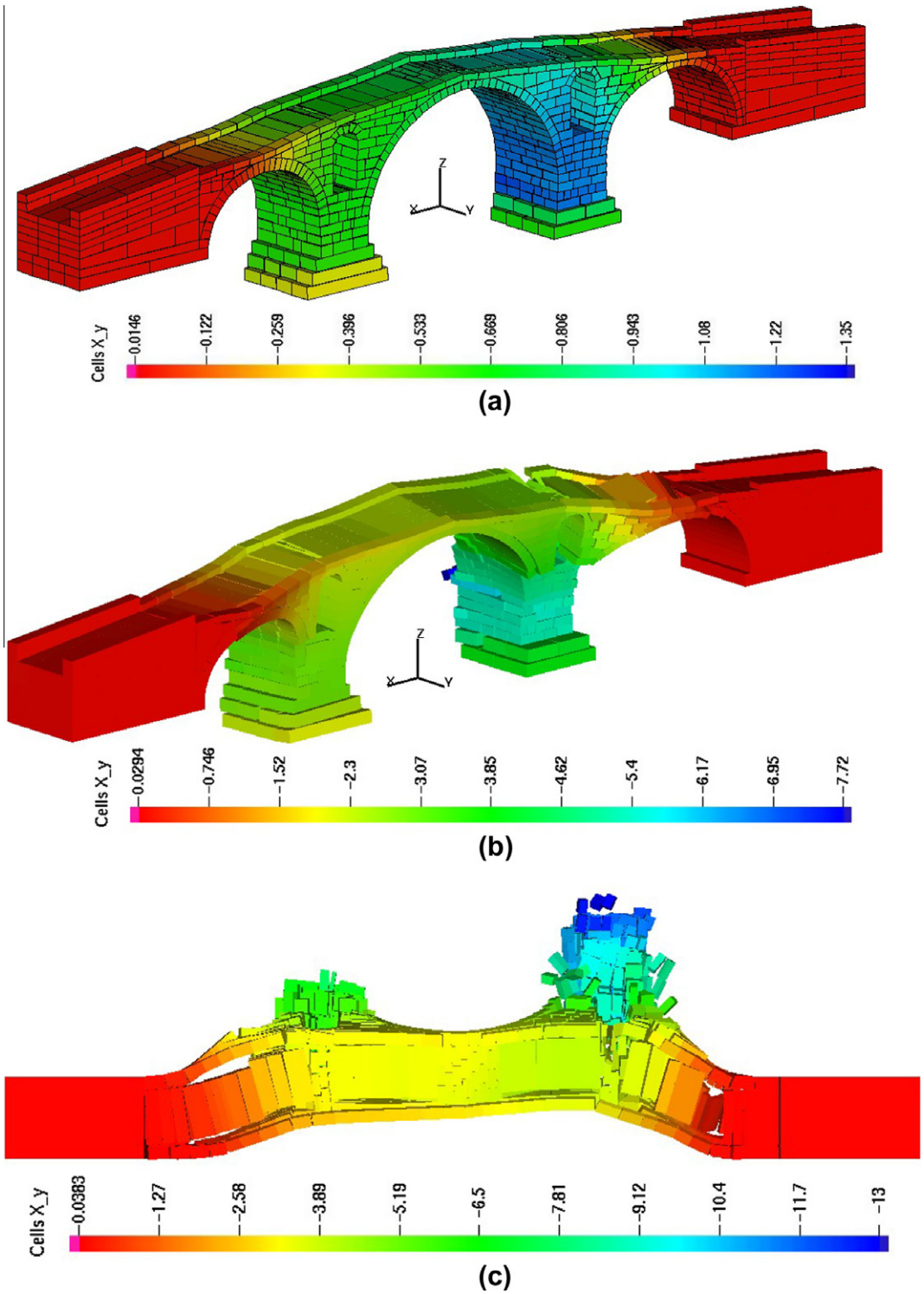

Fig. 8. Three snapshots of horizontal displacement in meter for the Julien bridge under lateral force applied on two central pillars: (a) at third second, (b) at 3.5th second and (c) view from above at 3.75th second.

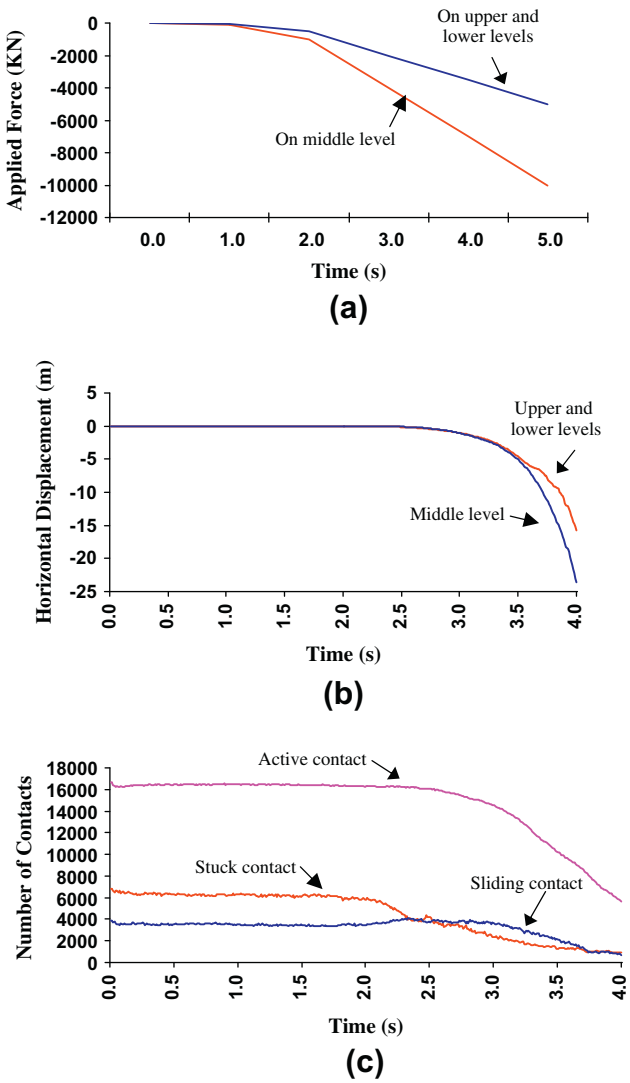

Fig. 9. (a) Change of the applied horizontal force (kN) over different levels of the two central pillars, (b) mean horizontal displacements (in the *Y* direction, see Fig. 8) in meter on three levels of the pillars, and (c) change in the number of contacts: sliding, stuck and all active contacts.

density. It should be noted that all these parameters are not taken into account in detail in the current study.

Before beginning to investigate the mechanical behaviour of the bridge under quasi-static loading, the static state of the bridge is studied in 3D and 2D models. The results presented in Fig. 7 show the state of this bridge under a static condition for 2D rigid and deformable models extracted from the 3D geometrical model. The contact conditions considered in these models are a dry friction contact with 0.7 for the friction coefficient between the masonry blocks, and 0.9 between the blocks and the ground. The mechanical properties of the stone blocks are presented in Table 1. The number of blocks in the 2D rigid model is 351 under dry friction contact. Fig. 7a shows the results obtained for the vertical displacement of the roman bridge under its own weight.

For the 2D deformable state, these 351 discrete blocks are meshed into 13,118 triangular elements (Fig. 7b and c). As can be observed, the vertical displacements of the bridge under self weight condition for the 2D rigid model are really negligible (Fig. 7a); while for the deformable model (Fig. 7b) the vertical displacements are increased. It seems that much of the vertical displacement in this case is caused by the block deformation. The mechanical parameters were extracted from the laboratory work performed by Delphine Raffard during her PhD [27]. The assessment of the bridge behaviour, as a structure, should be viewed as an academic assessment of a method and not as an engineering assessment of the actual resistance of a masonry stone bridge under real flood conditions.

In addition, this roman bridge is studied for a condition in which one or two central pillars are displaced for example by a flood force. In order to be able to model the flood condition, an incrementally increasing force with time is imposed over the central pillars in the 3D model. The snapshots of Fig. 8 illustrate the state of the roman bridge under lateral forces applied on its two central pillars. The applied horizontal forces at the middle level of the pillars increase differently in comparison with the forces applied on the upper and lower levels. The graph in Fig. 9a shows the trend of force change for each level during 5 s. As can be seen much more force is applied over the middle level of two central pillars. Remembering that each level is 2 m high, the maximum pressure over the middle levels of the pillars at the end of loading (5th second) will raise approximately to 1 MPa. Under these increasing horizontal forces, the bridge remains stable for nearly the first 2 s, then, its failure begins. As can be observed in Fig. 8 the right pillar begins to move earlier than left one, however the applied force is similar on both pillars. This issue can be obviously seen in Fig. 8c.

The mean horizontal displacement for each level of the central pillars is illustrated in Fig. 9b, which shows that the middle levels of the central pillars are moved faster than the two other levels, see also Fig. 8b. On the basis of their nature, the number of contacts is recorded during the calculation time and the results are shown in Fig. 9c. As can be seen in this graph the number of stuck contacts decreases after the 2nd second and the number of active contacts also decreases gradually due to block detachments occurring inside the model. The number of sliding contacts becomes greater than the number of stuck contacts after the beginning of failure.

The failure mechanism of the bridge is also investigated in the case of lateral loading only applied on the right central pillar. Fig. 10 illustrates the obtained results for this state; the loading trend and magnitude are the same as in Fig. 8. The right central pillar is subjected to lateral forces at three levels: the force in the middle level is greater than the force applied on the two other levels Fig. 9a. The instability and failure inside the model start after the 2nd second and the number of different types of contacts is changed in a way similar to the previous case, i.e. the loading on the two central pillars (Fig. 10c).

Finally the bridge model is also studied under uniform lateral loading condition, both for the loading case on two central pillars and only the right central pillar. In other words, the applied force is considered to be uniform on three levels and this force is equal to the force applied to the middle level in the precedent models. Fig. 11 shows the state of the bridge for two conditions including loading on two central pillars (Fig. 11a) and on the right central pillar (Fig. 11b). As can be seen, the whole lower part of the pillars is moved under uniform loading in both cases. Fig. 11a illustrates that the right pillar again moves faster than the left one. This suggests the relative weakness of this pillar against lateral loading which can be due to a different arrangement of the blocks, on this pillar.

4. Conclusion

The Non-Smooth Contact Dynamics method (NSCD) is applied in the current study to investigate the possible failure mechanisms of the stone masonry arches under different loading conditions. This numerical method by considering its important characteristic

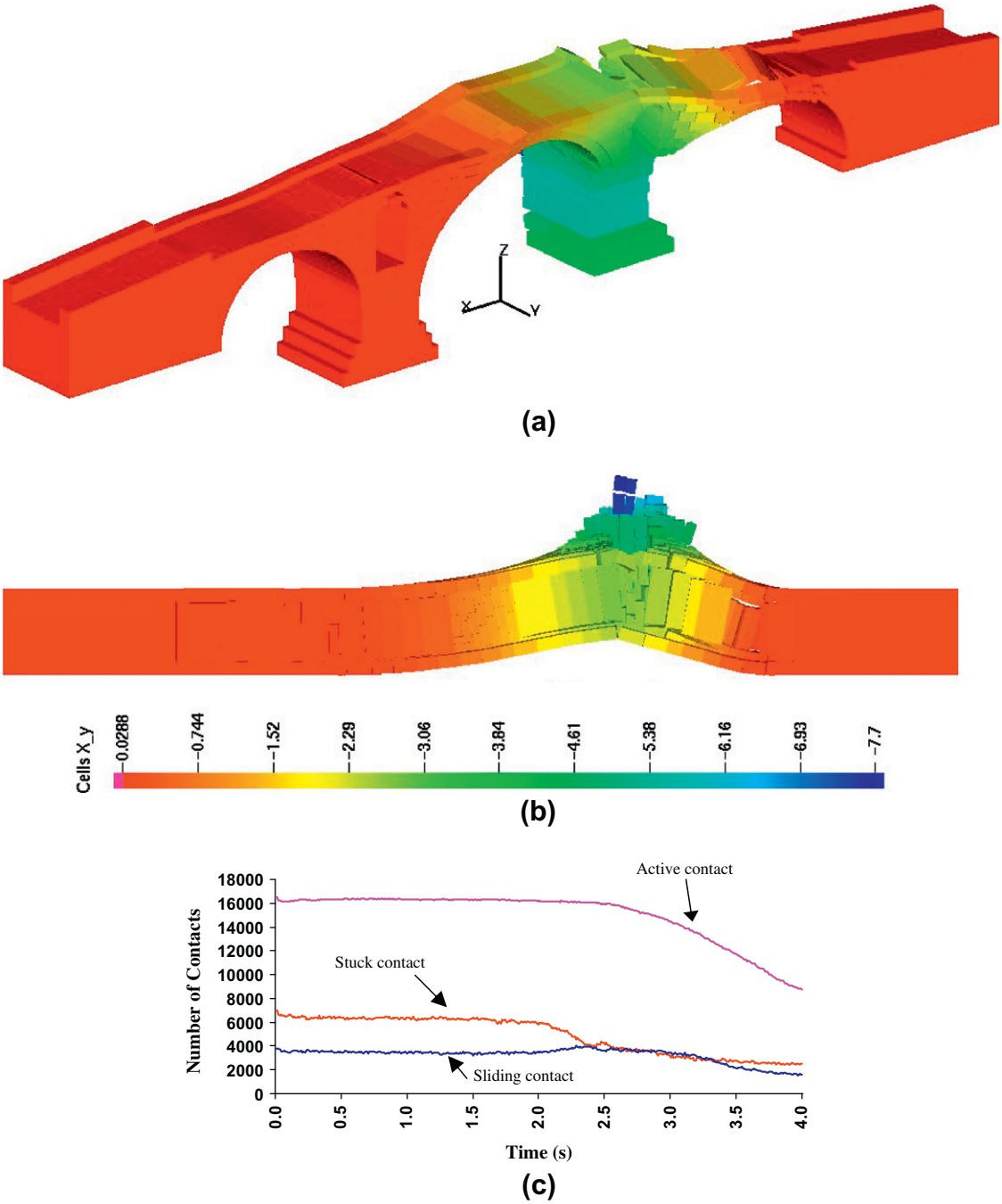

Fig. 10. (a and b) Results obtained for the Julien bridge under lateral force applied on the right central pillar at 3.5th second of the calculation time and (c) change in the number of contacts, including sliding, stuck and all active contacts.

of resolving frictional contact problems without introducing artificial penalization parameters or damping, as demonstrated by different models, can be an efficient tool to study the complex masonry structure behaviour under diverse loading conditions. At the first step of the study, a single-span arch bridge is investigated under vertical static loading imposed at the quarter of its span, the obtained results for failure mechanism is consistent with the analytical method results. The classic arch shows the four hinge failure mechanism in two and three dimensional analysis. This is a classical qualitative result that can be found in Heyman [29], pp. 17, 19, and 21. A more detailed discussion on this topic can be found in [30].

In addition, a roman stone bridge, as a full-scale test, is studied under lateral loading conditions, as can be the case during floods. This condition is simulated by applying an incremental force increasing with time having different trends, for several levels of the central pillars. The applied force increases until the pillars become instable and the failure of bridge begins. Different failure mechanisms are investigated by changing the loading procedure, and in this way the weaker parts of the bridge are determined. This type of loading does not simulate in a realistic way the flooding condition due to its high complex nature and the large number of changing factors which should be taken into account, see [31] for details. However, the results obtained demonstrate the capabil-

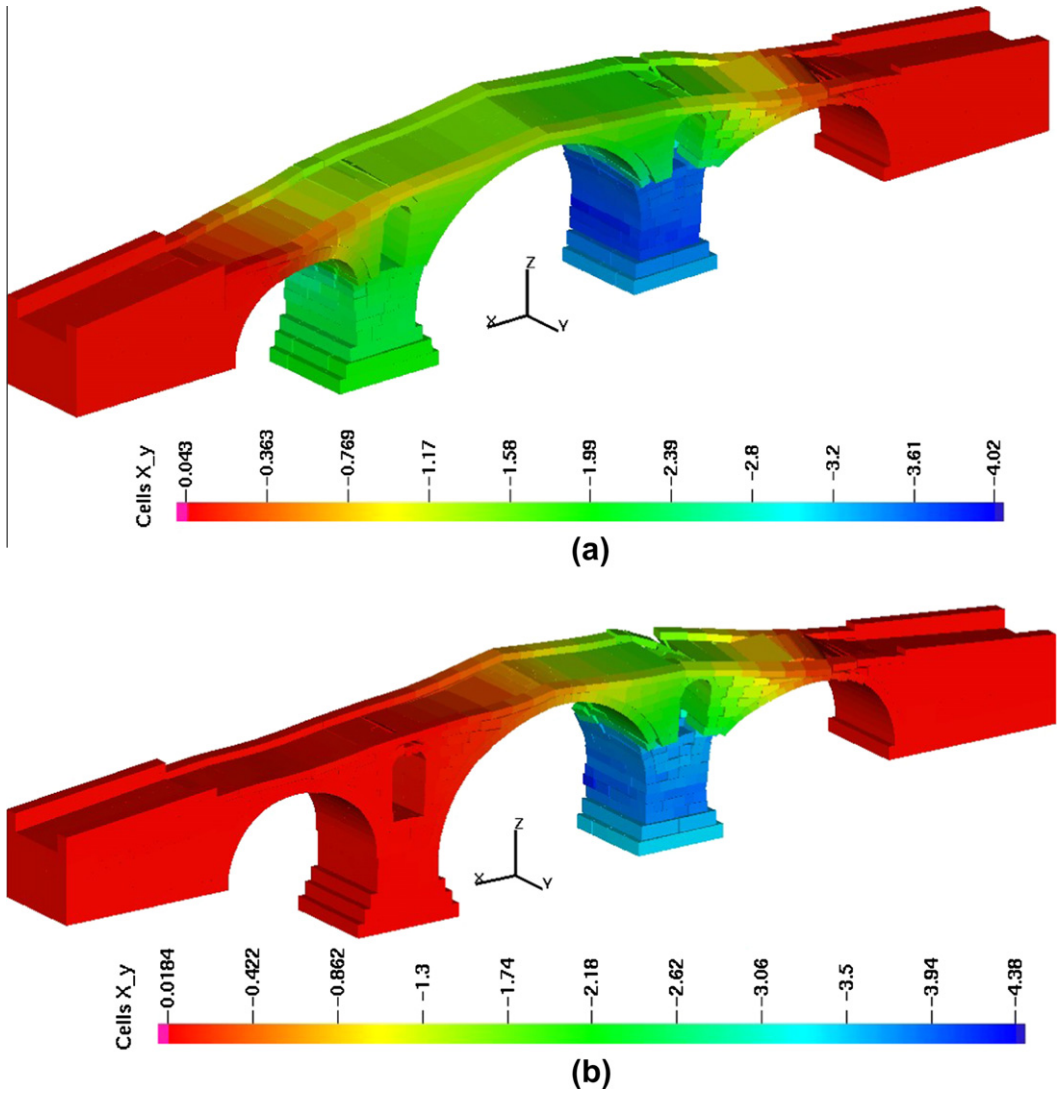

Fig. 11. Horizontal displacement in meter at third second of the calculation time for the Julien bridge under lateral force applied (a) on two central pillars and (b) on the right central pillar.

ity of the LMGC90 code based on NSCD method, to correctly assess the mechanical behaviour of the 3D masonry model, integrating the complex geometry of the actual blocks in the original structure.

Acknowledgements

The authors are grateful to Frédéric Dubois from the "Laboratoire de Mécanique et Génie Civil de Montpellier, France" for his valuable remarks on the NSCD method and especially on the LMGC90 code.

References

[1] Tóth AR, Orbán Z, Bagi K. Discrete element analysis of a stone masonry arch. Mech Res Commun 2009;36:469–80.

[2] Fanning PJ, Boothby TE. Three-dimensional modelling and full-scale testing of stone arch bridges. Comput Struct 2001;79:2645–62.

[3] Lourenço PB, Krakowiak KJ, Fernandes FM, Ramos LF. Failure analysis of Monastery of Jerónimos, Lisbon: how to learn from sophisticated numerical models. Eng Fail Anal 2007;14(2):280–300.

[4] Pelà L, Aprile A, Benedetti A. Seismic assessment of masonry arch bridges. Eng Struct 2009;31:1777–88.

[5] Drosopoulos GA, Stavroulakis GE, Massalas CV. Limit analysis of a single span masonry bridge with unilateral frictional contact interfaces. Eng Struct 2006;28:1864–73.

[6] Chetouane B, Dubois F, Vinches M, Bohatier C. NSCD discrete element method for modelling masonry structures. Int J Numer Methods Eng 2005;64:65–94.

[7] Thavalingam A, Bicanic N, Robison JI, Ponniah DA. Computational framework for discontinuous modelling of masonry arch bridges. Comput Struct 2001;79:1821–30.

[8] Orduna A, Lourenco PB. Three-dimensional limit analysis of rigid blocks assemblages. Part I: torsion failure on frictional interfaces and limit analysis formulation. Int J Solids Struct 2005;42:5140–60.

[9] Orduna A, Lourenco PB. Three-dimensional limit analysis of rigid blocks assemblages. Part II: load-path following solution procedure and validation. Int J Solids Struct 2005;42:5161–80.

[10] Oliveira DV. Experimental and numerical analysis of blocky masonry structures under cyclic loading. PhD thesis, University of Minho, Guimaraes, Portugal; 2003. <http://www.civil.uminho.pt/masonry>.

[11] Dubois F, Jean M. LMGC90 une plateforme de développement dédiée à la modélisation des problèmes d'interaction. In: Actes du sixième colloque national en calcul des structures. CSMA-AFM-LMS; 2003. p. 111–8.

[12] Jean M. Unilateral contact and dry friction: time and space variables discretization. Arch Mech Warszawa 1988;40(1):677–91.

[13] Jean M. Frictional contact in rigid or deformable bodies: numerical simulation of geomaterials. Amsterdam: Elsevier Science Publisher; 1995. p. 463–86.

[14] Jean M. The non-smooth contact dynamics method: special issue on modelling contact and friction. Comput Methods Appl Mech Eng 1999;177:235–57.

[15] Jean M. Micromécanique des matériaux granulaires. In: Hermes, editor. Chapter simulation numérique discrète. Paris; 2001. p. 199–324.

[16] Jean M, Moreau JJ. Unilaterality and dry friction in the dynamics of rigid body collections. In: Proceedings of contact mechanics international symposium. Presses Polytechniques et Universitaires Romandes, Lausanne, Switzerland; 1992. p. 31–48.

[17] Moreau JJ. Unilateral contact and dry friction in finite freedom dynamics. International centre for mechanical sciences, courses and lectures, vol. 302. Vienna: Springer; 1998. p. 1–82.
[18] Moreau JJ. New computation methods in granular dynamics. In: Powders and grains, vol. 93. Rotterdam: A.A. Balkema; 1993. p. 227–32.
[19] Moreau JJ. An introduction to unilateral dynamics. In: Frémond M, Maceri F, editors. Novel approaches in civil engineering, number 14 in lecture notes in applied and computational mechanics. Springer-Verlag; 2004. p. 1–46.
[20] Topina V, Dubois F, Monerie Y, Perales F, Wachsd A. Micro-rheology of dense particulate flows: application to immersed avalanches. J Non-Newton Fluid Mech 2011;166:63–72.
[21] Jean M, Moreau JJ. In: Blanc R, Suquet P, Raous M, editors. Dynamics of elastic or rigid bodies with frictional contact and numerical methods. Vienna: Publications du LMA; 1991. p. 9–29.
[22] Radjai F, Richefeu V. Contact dynamics as a nonsmooth discrete element method. Mech Mater 2009;41:715–28.
[23] Rafiee A, Vinches M, Bohatier C. Modelling and analysis of the Nimes arena and the Arles aqueduct subjected to a seismic loading, using the Non-Smooth Contact Dynamics method. Eng Struct 2008;30:3457–67.
[24] Acary V, Blaise JY, Drap P, Florenzano M, Garrec S, Jean M, et al. NSCD method applied to mechanical simulation of masonry in historical buildings using MOMA. In: XVII CIPA (international committee for architectural photogrammetry) international symposium WG3—simple methods for architectural photogrammetry. Olinda, Brazil; 1999.
[25] Rafiee A, Vinches M, Bohatier C. Application of the NSCD method to analyse the dynamic behaviour of stone arched structures. Int J Solids Struct 2008;45:6269–83.
[26] Rafiee A. Contribution to the study of fractured rock masses: characterization of the in situ fracture network, geostatistics and discrete element modelling. PhD thesis, University of Montpeiller II; 2008. 273p.
[27] Raffard D. Modélisation de structures maçonnées par homogenisation numérique non-linéaire: application aux ouvrages d'intérêt archéologique = Numerical Modelling of old masonry using non-linear homogenization. PhD thesis, Institut national polytechnique de Lorraine; 2000. 206p.
[28] Hulet KM, Smith CC, Gilbert M. Load-carrying capacity of flooded masonry arch bridges. Bridge Eng 2006;159:97–103.
[29] Heyman J. The stone skeleton. Cambridge University Press; 1995. ISBN: 0-521-62963-2.
[30] Como M. Statica delle costruzioni storiche in muratura. Archi, volte, cipole, architetture monumentali, edifici sottocarichi verticali e sotto sisma, ARACNE Editrici; 2010. p. 161 and following pages.
[31] Kallaka T, Wang C-J. Efficient numerical model for studying bridge pier collapse in floods. World Acad Sci Eng Technol 2011;60:1011–6.